Effect of Milling of V_2O_5 on the Local Environment of Vanadium as Studied by Solid-State ^{51}V NMR and Complementary Methods

A. A. Shubin,[†] O. B. Lapina,[†] E. Bosch,[‡] J. Spengler,[‡] and H. Knözinger*[,‡,§]

Boreskov Institute of Catalysis, Pr. Akad. Lavrentieva 5, Novosibirsk 630090, Russia, and Institut für Physikalische Chemie, Universität München, Sophienstr. 11, 80333 München, Germany

Received: November 23, 1998; In Final Form: February 16, 1999

Milling of V_2O_5 in a ball mill increased the surface area from 7 to a maximum of 32 m^2/g. Simultaneously, XRD line broadening suggested a reduction of the microcrystallites. A color change during milling indicated oxygen loss, and Raman spectroscopy provided evidence for the formation of shear structures such as V_6O_{13}. The number of V^{4+} ions produced was determined by ESR spectroscopy and that of V^{3+} ions was obtained from magnetic susceptibility measurements. The local environment of the vanadium nucleus in V_2O_5 after milling in a ball mill was characterized by the combination of static (wide line) and MAS ^{51}V NMR techniques together with theoretical simulations of NMR spectra. Important information on the quadrupole and chemical shielding tensors, including the relative tensor orientation and the distribution of magnetic resonance parameters, is discussed for the vanadium nucleus in V_2O_5 after milling. Special attention was given to the formation of paramagnetic V^{3+} and V^{4+} ions and their influence on ^{51}V NMR spectra of diamagnetic V^{5+} in milled samples. It was shown that paramagnetic V^{3+} ions are responsible for the loss (up to about 70%) of the intensity in ^{51}V NMR spectra. The influence of other V^{4+} paramagnetic ions is significantly smaller.

Introduction

In addition to the traditional methods for preparation of vanadia-based catalysts such as impregnation, coprecipitation, and grafting, an alternative process, namely, the milling of the powder components in a ball mill, was also used in recent years.[1−4] To describe the mechanism of the interaction between two (or more) solids, detailed knowledge of the interfaces between them is necessary. Thus, for instance, Haber and coworkers have strongly emphasized the role which surfaces and interfaces play in the reactivity of solids.[5−7] The thermal spreading of a solid on the surface of another solid was described as a solid−solid wetting phenomenon, as reviewed by Knözinger and Taglauer.[4,8] In addition to the simultaneous grinding of two oxide powders, the milling of only one of them (supported oxide) with subsequent calcination of the mixture was also used for catalysts preparation.[9] To understand the mechanism of oxide/oxide interactions in this case, the effects of milling of pure oxides must be understood in detail. During the grinding procedure, the grain sizes and grain-size distributions of the solid oxide are changed[10,11] and the resulting dispersity is known to be important for the reactivity of powder mixtures.[10] In the present work, we aim at understanding the changes in the local environment of nuclei in pure oxides induced by ball milling. As an example, V_2O_5, the active component of vanadia-based catalysts, was used. ^{51}V NMR seems to be the most suitable technique for the characterization of V^{5+} sites since this method provides valuable information on the local environment of the vanadium nucleus.[12−14] Some new NMR techniques developed in recent years (such as SATRAS,[15−19] MQ-MAS,[20−23] etc.) permit in some cases the extraction from solid-state NMR measurements of complete information on chemical shielding tensor and quadrupolar tensor parameters which may be used for the description of the local environment and its distortions for the nuclei under NMR study. Additionally, ESR and magnetic susceptibility methods were used for the characterization of paramagnetic V^{4+} and V^{3+} species that are formed during milling. Surface area measurements, X-ray diffraction (XRD), and Raman spectroscopy provided additional structural and morphological information.

Experimental Section

Vanadium oxide V_2O_5 was from J. T. Baker Chemicals B. V. and had a purity of >99%. V_2O_5 has a density of 3.36 g/cm^3. Into an agate vessel (250 cm^3 volume) was placed 60 g of V_2O_5 together with six agate balls (1.5 cm diameter, 11 g), and this was milled for up to 20 h at approximately 150 revolutions per minute. Samples were taken after 3, 10, and 20 h for analysis.

For the measurement of BET surface areas, samples were evacuated at 200 °C and 4×10^{-2} mbar. N_2 adsorption isotherms were measured on a Sorptomatic 1800 (Carlo Erba) which was controlled via the software Mileston 200. Specific surface areas S_{BET} were calculated from the experimental data in the range of relative pressures of $0.05 \leq p/p_o \leq 0.35$ (p_o = N_2 saturation pressure at liquid N_2 temperature). Average particle diameters d were calculated from the equation

$$d = 6/(S_{BET}\,\rho)$$

where ρ is the bulk density of the oxide. X-ray powder patterns were obtained using Cu K_α radiation.

Laser Raman spectra were recorded on a Dilor OMARS-89 spectrometer at a spectral resolution of 5 cm^{-1}. The spectrometer was equipped with a CCD camera (1752 × 532 Pixel) from Princeton Instruments. The 514 nm line of an Ar^+ ion laser model 2020 of Spectra Physics was used for excitation at a laser power of 20 mW at the sample position. Spectra were recorded

[†] Boreskov Institute of Catalysis.
[‡] Universität München.
[§] Current address: Universität München, Institut für Physikalische Chemie, Butenandtstrasse 5-13 (Haus E), 81377 München, Germany.

10.1021/jp984513s CCC: $18.00
Published on Web 04/03/1999

TABLE 1: BET Surface Areas and Average Particle Diameters for Milled V_2O_5 Samples

milling time/h	S_{BET}/m^2g^{-1}	d/nm
0	7	252
3	17	105
10	32	56
20	21	83

in the backscattering mode using the scanning multichannel technique (SMT) for improving the signal-to-noise ratio.

^{51}V NMR measurements were made on a Bruker MSL-400 spectrometer ($\nu_0 = 105.25$ MHz for the ^{51}V resonance) using spin−echo and one-pulse (wide line and MAS NMR) techniques. MAS spectra of powders were recorded for samples rotating at frequencies from 2 to 10 kHz using a 5 mm rotor and the NMR probe constructed by Jakobsen et al.[24] Quadrupolar echo experiments were performed with the two-pulse sequence: $\{\pi/12(X) - t_1 - \pi/12(Y) - t_2\}$, where t_1 and t_2 were chosen empirically to be near 55 μs and 57 μs, respectively. Repetition times from 0.1 to 2 s and rf pulses with a duration of ~1 μs were used in the experiments. The distortions of NMR spectra resulting from the incomplete spectrum excitation by rf pulses and due to the NMR probe Q-factor were minimized by recording the spectra with different frequency offsets and applying subsequent numerical corrections. This procedure was necessary for the quantitative analysis of MAS NMR data with the SATRAS technique.[16] All chemical shieldings are referenced to $VOCl_3$ as an external standard. For better phasing and for minimizing baseline distortions in the NMR spectra, the linear prediction (backward LP-SVD analysis) of the first few (2−6) free induction decay data points and, in evident cases, polynomial baseline corrections were used.

Simulations of ^{51}V static and MAS NMR spectra were performed taking into account the second-order quadrupole effects and using the general purposes NMR1 program.[25] A particular variant of this program especially adopted to the fast computation of spinning sideband (ssb) intensities in MAS experiments (Herzfeld and Berger approach)[26] was used for SATRAS simulations and least-squares fits of ssb intensities. Computations were performed on a dual Pentium II 300 MHz based PC and SUN SparcStation10 equipped with four 90 MHz ROSS Hyper Sparc CPUs.

The ESR spectra were recorded on a Varian E-Line (E9) spectrometer with a microwave frequency of 9.2 GHz. For exact intensity determinations the samples were measured in a double cavity resonator against a $CuCl_2$ single crystal as a standard. The magnetic susceptibility measurements were carried out using a home-built magnetic balance.

Results and Discussions

BET Surface Areas. BET surface areas and average particle sizes of V_2O_5 samples as they develop with increasing milling time are summarized in Table 1. The as-received V_2O_5 sample has a small surface area of 7 m^2/g and correspondingly large average particle sizes of ca. 250 nm. Milling for 3 h leads to crushing of these particles; the surface area increases to 17 m^2/g, and the particle size drops to ca. 105 nm. The highest surface areas, namely 32 m^2/g, and smallest particle sizes (ca. 56 nm) were obtained after 10 h milling. For longer milling times, namely 20 h, reagglomeration of small particles occurs as indicated by a reduction of surface area to 21 m^2/g and an increase of the average particle size to ca. 80 nm.

Laser Raman Spectra. No vanadium oxide phases other than V_2O_5 could be detected by XRD even for the 20 h milled sample. However, significant line broadening was observed which is induced by the decreased crystallite sizes and formation of structural defects during milling.

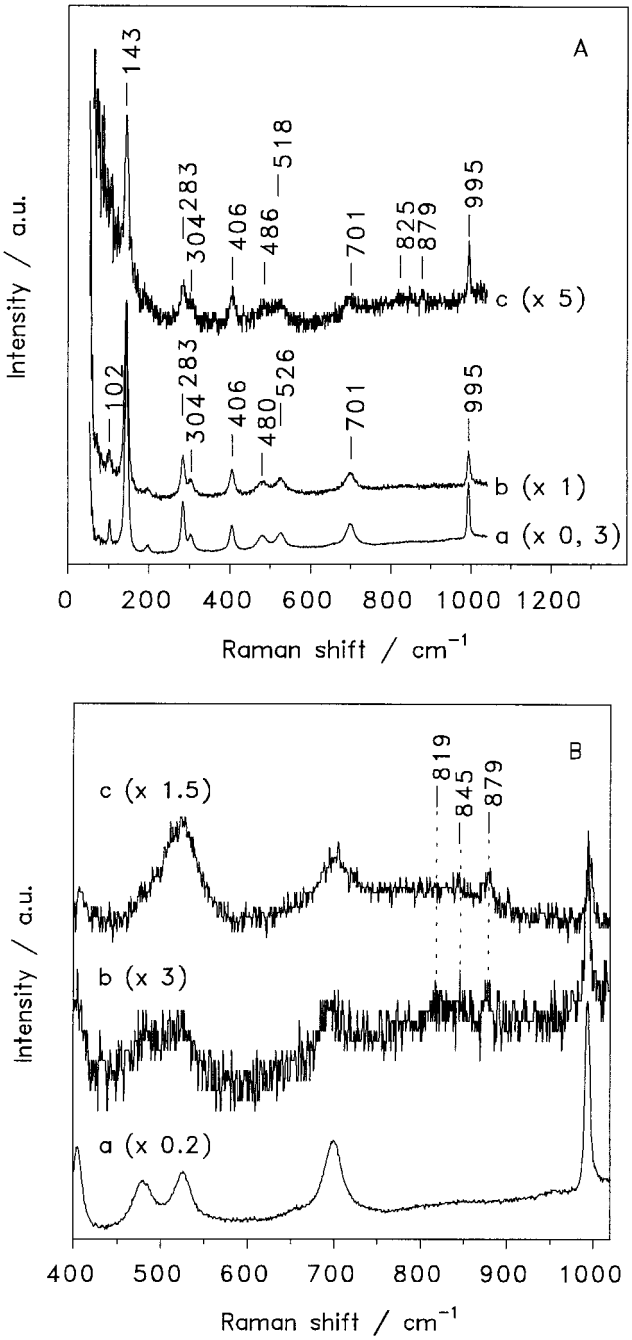

Figure 1. Laser Raman spectra of vanadium oxide samples: (A) (spectrum a) V_2O_5, as received, (spectrum b) V_2O_5 after 10 h milling, (spectrum c) V_2O_5 after 20 h milling; (B) (spectrum a) V_2O_5, as received, (spectrum b) V_2O_5 after 20 h milling; (c) V_6O_{13}.

Figure 1A shows the Raman spectra of V_2O_5 as they develop with increasing duration of milling. The spectrum of the sample after 10 h milling exhibits all characteristic vibrational features of polycrystalline V_2O_5 (spectrum a), although the signal-to-noise ratio is reduced in spectrum b. This is related to a visible color change from light yellow to a deeper yellow, suggesting partial reduction via oxygen loss during milling to form V_2O_{5-x}. The signal-to-noise ratio further decreases after 20 h milling (spectrum c) when the sample color has turned to green. The frequency range 400−1000 cm^{-1} for as-received polycrystalline V_2O_5 (spectrum a) and for authentic V_6O_{13} (spectrum c) is compared in Figure 1B with that of the V_2O_5 sample after 10

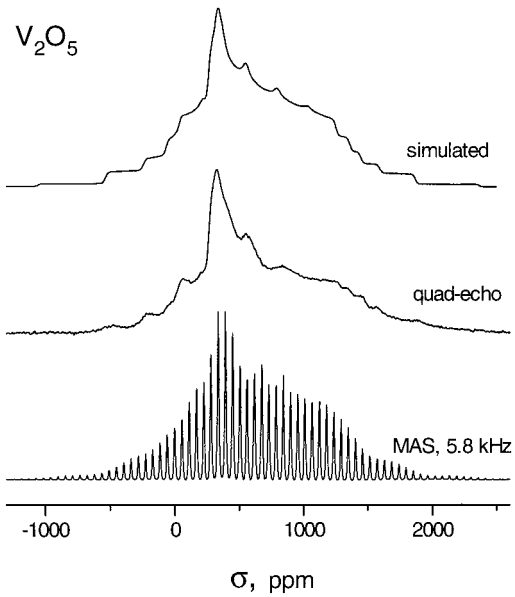

Figure 2. (a) 105.25 MHz ^{51}V MAS NMR spectrum of V_2O_5 at spinning frequency $\nu_r = 5.86$ kHz; (b) wide line quadrupolar echo recorded with $t_1 = 55$ μs and $t_2 = 57$ μs; (c) for comparison is shown a one-pulse spectrum simulated with data set 1 from Table 1.

h milling. The latter spectrum clearly still shows the characteristics of polycrystalline V_2O_5, although the vibrational bands are broadened. The V_2O_5 doublet at 480 and 526 cm^{-1} is poorly resolved in the milled sample and shows some similarity with the broad band at 523 cm^{-1} of V_6O_{13}. The weak features of V_6O_{13} at 845 and 879 cm^{-1} are also detectable in the milled sample. It is therefore inferred that the milling induces oxygen loss and most likely formation of shear structures comparable to V_6O_{13}. From the V^{3+} and V^{4+} concentrations reported below (Table 3), an average formal oxidation state of 4.8 can be calculated for vanadium in the sample after 20 h milling. As the formal oxidation state of vanadium in V_6O_{13} is 4.3, the milled sample may contain limited regions of V_6O_{13}-like shear structures besides a majority phase consisting of V_2O_5 (and/or V_2O_{5-x}) consistent with XRD and Raman spectra.

Nuclear Magnetic Resonance. Two typical (MAS and quad-echo) experimental spectra of the initial (as received) V_2O_5 sample along with a one-pulse simulated static NMR spectrum are shown on Figure 2. The quadrupole and magnetic shielding tensor parameters were determined from the simulations using the SATRAS technique, and the ssb intensities were obtained from MAS spectra at three different rotation frequencies (see Table 2). Note that NMR parameters obtained for V_2O_5 in this research are close to values reported in the literature.[15,18] The main difference is a slightly larger value of the quadrupole asymmetry parameter, namely, $\eta \approx 0.2$ as compared to reported values of $0 \leq \eta \leq 0.13$. Nevertheless, as may be seen from Figure 2, there is a good agreement for the position of characteristic features in the simulated one-pulse NMR spectrum and the experimental quad-echo spectra. This is independent confirmation for the accuracy of the parameters determined by the SATRAS method in this study.

When the vanadium oxide is subjected to milling, one should expect at least the appearance of additional distortions and defects in V_2O_5 microcrystals and, as a consequence, the presence of distribution of magnetic resonance parameters (components of chemical shielding and quadrupole tensors along with relative orientation of these tensors) with respect to as-received V_2O_5. To understand in more detail the influence of relatively small parameter variations on the observed ^{51}V NMR spectra, some simulations of one-pulse static and MAS spectra were performed. The results of these simulations are presented in Figures 3−7. Only Gaussian-like distributions of quadrupole coupling constants C_Q around the unperturbed value were used in the simulations of V_2O_5 NMR spectra. Certainly, the real distribution function should be more complex,[17] but for the small width of the distributions observed in the experiments and used in simulations it is almost impossible to discriminate between different model distributions for the quadrupole tensor components. As a rule, the use of C_Q distributions only is quite sufficient for the semiquantitative estimations. As expected, C_Q distributions with distribution parameters ΔC_Q of 150 or 300 kHz results in broadening of satellite transitions in the static NMR spectra with the loss of the corresponding high-field edge structure in spectra (Figure 3). Only the central transition remains unchanged because second-order quadrupolar effects are absent for this transition. As shown in Figure 4, C_Q distribution effects reveal themselves in MAS NMR spectra as systematic changes of integral intensities of ssb peaks and, therefore, these effects may also be estimated from the comparison of experimental and calculated MAS NMR spectra. Note that, according to our simulations, the static one-pulse NMR spectrum of V_2O_5 is more sensitive (in its high-field edge) to the ΔC_Q value than the corresponding MAS spectrum for ΔC_Q values below 100−150 kHz. Therefore, simulated static spectra are more suitable (if their quality is appropriate) for the estimation of ΔC_Q.

Figures 5 and 6 show the influence of distributions of selected principal values of the chemical shielding tensor or its isotropic value on the one-pulse spectra and on the MAS NMR spectra at low rotation frequency (2 kHz), respectively. As can be seen, 2 kHz MAS spectra (Figure 6) are significantly more sensitive to the small distributions of the chemical shielding tensor principal values than static NMR spectra (Figure 5). The main reason for this sensitivity is the choice of a low rotation frequency when the distance between adjacent spinning sidebands is comparable with the chemical shielding distribution.

TABLE 2: ^{51}V Quadrupole Tensor Parameters (C_Q, η_Q),[a] Chemical Shielding Tensor Parameters (δ_σ, η_σ, σ_{iso}),[b] and Euler Angles (α, β, γ) Describing the Relative Orientation of Quadrupole Tensor with Respect to Chemical Shielding Tensor for V_2O_5 from MAS NMR Measurements

ν_r (kHz)	no. of ssb[c]	C_Q (kHz)	η_Q	δ_σ (ppm)	η_σ	σ_{iso}	α (deg)[d]	β (deg)	γ (deg)[d]
5.860	74	799	0.22	635	0.09	612[e]	146	127	139
6.836	59	799	0.20	637	0.13		133	128	151
9.085	42	801	0.21	638	0.13		135	128	152

[a] Nuclear electric quadrupole moment eQ, electric field gradient tensor eigenvalues (V_{xx}, V_{yy}, and $V_{zz} = eq$) are connected with C_Q and η_Q by the relations: $C_Q = e^2qQ/h$; $V_{xx} = 1/2(-1 - \eta_Q)V_{zz}$; $V_{yy} = 1/2(-1 + \eta_Q)V_{zz}$. [b] The eigenvalues of chemical shielding tensor are expressed by δ_σ, η_σ, and σ_{iso} in the following manner: $\sigma_{xx} = 1/2\delta_\sigma(-1 - \eta_\sigma) + \sigma_{iso}$; $\sigma_{yy} = 1/2\delta_\sigma(-1 + \eta_\sigma) + \sigma_{iso}$; $\sigma_{zz} = \delta_\sigma + \sigma_{iso}$. [c] Number of spinning sideband intensities used in optimization. [d] Angles α and γ are determined with significant error because the symmetry of the chemical shielding tensor and quadrupole tensor is close to axial. [e] σ_{iso} was determined from the position of the zero spinning sideband and presented here without second-order quadrupole shift correction which is small (about 0.1 ppm) as compared to experimental errors.

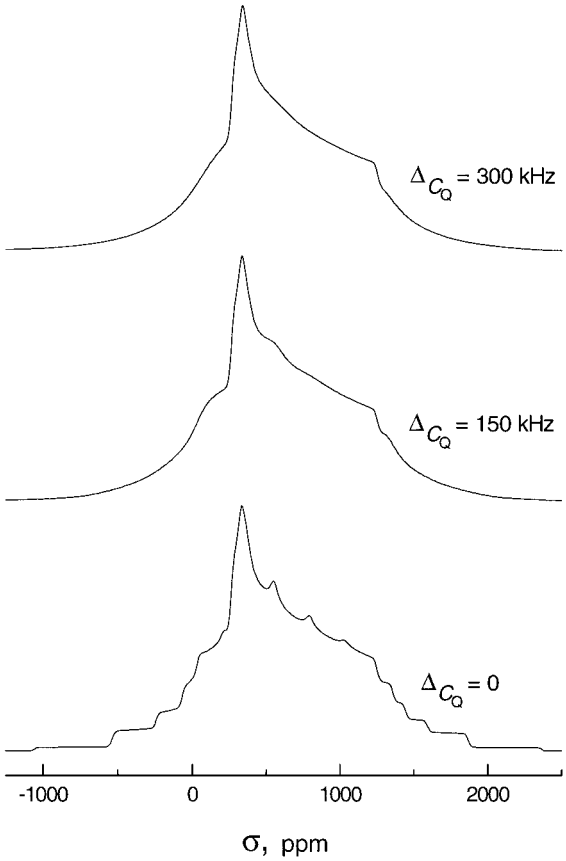

Figure 3. Simulated 105.25 MHz ^{51}V NMR one-pulse spectra of V_2O_5 using data set 1 from Table 1 and quadrupolar constant C_Q distributed around 799 kHz in a Gaussian-like fashion: (a) $\Delta C_Q = 0$; (b) $\Delta C_Q =$ 150 kHz; (c) $\Delta C_Q =$ 300 kHz. Individual NMR line width was Gaussian with $\Delta = 0.9$ kHz.

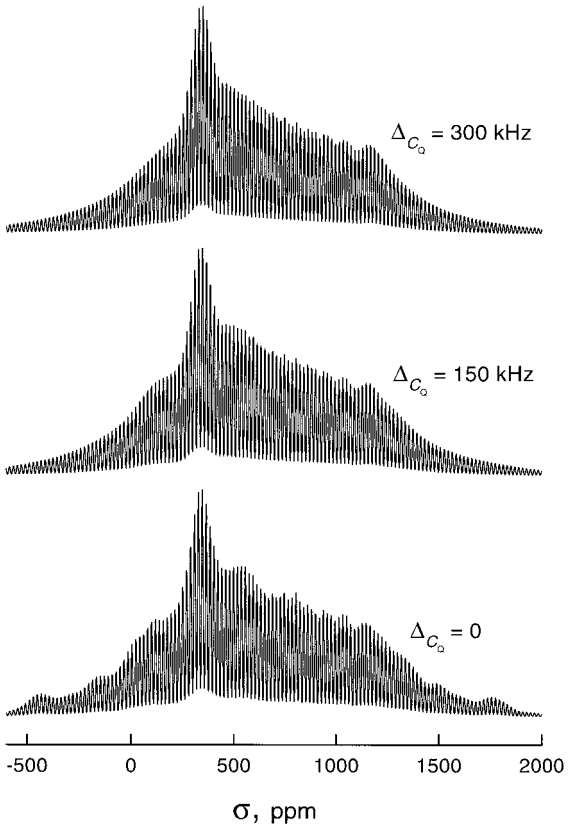

Figure 4. Simulated 105.25 MHz ^{51}V MAS NMR spectra of V_2O_5 at $\nu_r = 2.0$ kHz using data set 1 from Table 1 and quadrupolar constant C_Q distributed around 799 kHz in a Gaussian-like fashion: (a) $\Delta C_Q =$ 0; (b) $\Delta C_Q =$ 150 kHz; (c) $\Delta C_Q =$ 300 kHz. Individual NMR line width was Gaussian with $\Delta = 0.9$ kHz.

It is apparent from Figure 6, and may be easily appreciated from analytical expressions, that it is impossible to determine the principal value, the distribution of which is responsible for the changes in low-speed MAS NMR spectra. Certainly, the distribution of σ_{iso} is more pronounced, but for small $\Delta\sigma_{iso}$ the effect is the same as for distributions of any (σ_x, σ_y, σ_z) chemical shielding tensor component with a distribution width parameter of $3\Delta\sigma_{iso}$.

The influence of dry milling on the line shape of the static ^{51}V NMR spectra of pure V_2O_5 is shown in Figures 7 and 8. After 3 h of milling the satellite transition lines begin to blur. This effect is increased after longer milling times and a comparison with simulated spectra shows that a value of $\Delta C_Q \geq 150$ kHz for the quadrupole coupling constant distribution for the 20 h milled sample is a reasonable estimate. All ^{51}V MAS spectra of milled samples are characterized by only one set of spinning sidebands and the same value of the isotropic shift $\delta_{iso} = -612$ ppm. However, ssb intensities, their envelope, and a wide line in the bottom of the spectra are quite different for the various samples. Moreover, one can recognize a broad line in the MAS spectra (Figure 9) below the spinning sidebands even for the unmilled sample, originating in this case probably from the small overlap of adjacent ssb at 2 kHz sample rotation. This overlap is still not big enough to destroy the rotation structure. An increase of overlap can be clearly seen after 10 h and especially after 20 h of milling. Comparing the MAS spectra measured at different rotation frequencies (Figures 9 and 10) one can see that ssb overlap is clearly produced only at 2 kHz MAS while being negligible at 10 kHz.

In discussing the appearance of the broad line in ^{51}V NMR spectra the possible presence of paramagnetic V^{3+} and V^{4+} ions in milled V_2O_5 samples must also be taken into account. Dipole−dipole interactions between the magnetic moment of the V^{5+} nucleus and the magnetic moment of paramagnetic ions may result in NMR signal broadening and even in its disappearance. The relative amount of paramagnetic V^{4+} ions was estimated from ESR measurements using double integration of the first derivative absorption line (Table 3). As this procedure includes a significant uncertainty concerning the definition of the real baseline, it can only be used as a rough estimate. In principle ESR spectra contain information about the spatial distribution of the paramagnetic species. Paramagnetic centers in close vicinity can broaden ESR lines to such an extent that no hyperfine structure is resolved any more. A clearly resolved hyperfine structure representing the symmetry around the V^{4+} ion can only be detected for the supported samples. V^{3+} does not produce an ESR signal, neither at ambient nor at liquid nitrogen temperature.[27] Very short electron spin−spin and spin−lattice relaxation times are the most probable reason for this behavior. The amount of V^{3+} ions was therefore determined by magnetic susceptibility measurements.

The amounts of both V^{4+} and V^{3+} ions, as well as the relative peak intensity of the central transition in the static ^{51}V NMR spectrum, are listed in Table 3. The most striking observation following from a comparison of these data is the significant decrease in NMR signal intensity of the central transition for milled V_2O_5 samples (about 4 times for 20 h milled V_2O_5 as compared to the unmilled sample). Several mechanisms may be proposed for this phenomenon. First, there is the possibility of dipole−dipole interaction of V^{5+} ions with (V^{4+} or V^{3+})

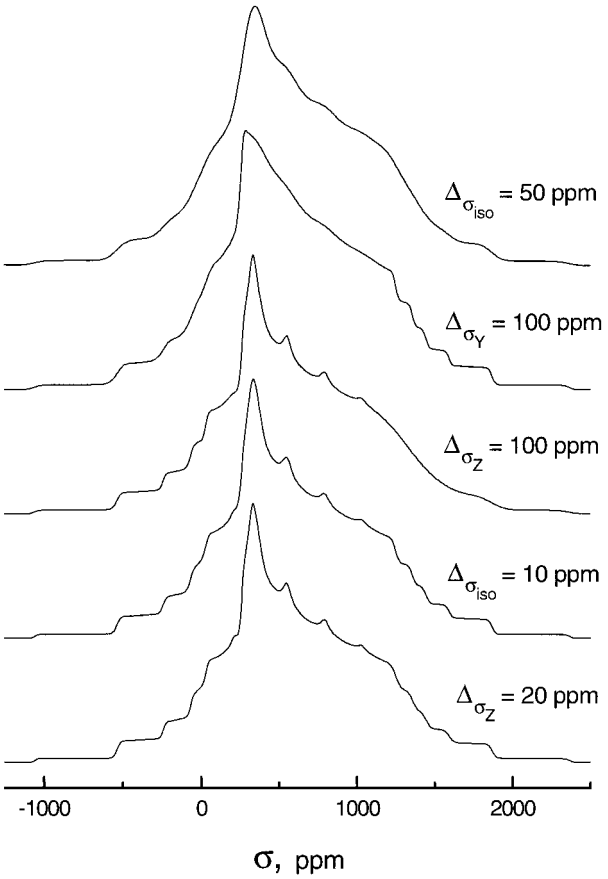

Figure 5. Simulated 105.25 MHz ^{51}V NMR one-pulse spectra of V_2O_5 using data set 1 from Table 1 and $\Delta\sigma$ distributed around its initial value in a Gaussian-like fashion: (a) $\Delta\sigma_z = 20$ ppm; (b) $\Delta\sigma_{iso} = 10$ ppm; (c) $\Delta\sigma_z = 100$ ppm; (d) $\Delta\sigma_y = 100$ ppm; (e) $\Delta\sigma_{iso} = 50$ ppm. Individual NMR line width was Gaussian with $\Delta = 0.9$ kHz.

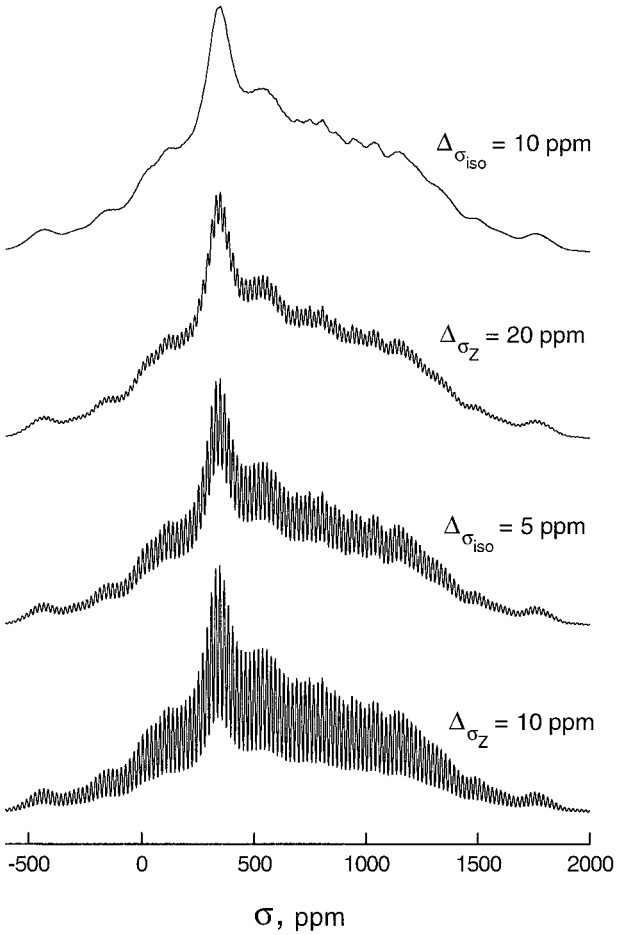

Figure 6. Simulated 105.25 MHz ^{51}V MAS NMR spectra of V_2O_5 at $\nu_r = 2$ kHz using data set 1 from Table 1 and $\Delta\sigma$ distributed around its initial value in a Gaussian-like fashion: (a) $\Delta\sigma_z = 10$ ppm; (b) $\Delta\sigma_{iso} = 5$ ppm; (c) $\Delta\sigma_z = 20$ ppm; (d) $\Delta\sigma_{iso} = 10$ ppm. Individual NMR line width was Gaussian with $\Delta = 0.9$ kHz.

paramagnetic ions in close vicinity. Assuming homogeneous spatial distribution of paramagnetic ions in the sample, a monotonic increase of individual line widths in ^{51}V NMR spectra with an increase of the concentration of paramagnetic ions is expected. Experimentally, however, the observerd NMR line widths are almost the same for the unmilled V_2O_5 and for the 10 h milled sample (which has the same V^{4+} concentration as the unmilled sample and about 2 times higher content of V^{3+} than unmilled V_2O_5), while the central NMR transition intensity for the 10 h milled sample is about 2 times smaller. In the case of a homogeneous spatial distribution we should receive not only global broadening resulting in a loss of intensity but also an intermediate broadening according to different distances from V^{5+} to paramagnetic ions. As the spectrum is only slightly broadened after 20 h milling there must be some inhomogeneity in the distribution of the paramagnetic vanadium atoms. This is confirmed by ESR measurements, in which no hyperfine structure is resolved consistent with the local formation of V_6O_{13}-like shear structures. On the other hand, the milling process which leads to the formation of V^{3+} and V^{4+} and, most likely to additional other defects, may also produce distributions of the quadrupole coupling constant, which results in a blurring of the characteristic peaks of all the transitions (including the central one). The latter is demonstrated in quad-echo spectra, represented in Figure 8. In principle, a detailed analysis of the spin−echo decay and its dependence on excitation conditions may provide valuable information on the magnetic resonance parameters (including dipolar interaction).[28,29] In the present case, the sensitivity of the NMR probe and instrumental instabilities did not allow systematic spin−echo measurements to be performed for all the samples. For this reason, the experimental conditions (rf pulse duration and amplitude) were chosen such that the spin−echo spectrum of as received V_2O_5 was as close as possible to its one-pulse spectrum. Identical experimental conditions were used in all measurements. The observed spectra do not give quantitative information. They reflect only the possible tendency of formation of a broad line in the bottom of static quad-echo NMR spectra of milled samples which contain high amounts of V^{5+} ions. This tendency is not as pronounced as it may appear from Figure 8, because the broad line in the bottom of the static quad-echo NMR spectrum of the 20 h milled sample is observed against the central transition with its amplitude being reduced to 27% of those for unmilled V_2O_5 (Table 3).

An analysis of the experimental data presented in Table 3 clearly indicates that there is a correlation between the concentration of paramagnetic V^{3+} ions in the sample and the intensity of the central NMR transition for diamagnetic V^{5+}. This is demonstrated in Figure 11 where the NMR intensity of the central transition is plotted against the V^{3+} concentration. In contrast, no correlation is evident between the concentration of V^{4+} paramagnetic ions and the NMR signal intensity. From the initial slope of about -5×10^{-21} g of the curve in Figure 10 and using 3.36 g/cm^3 as the V_2O_5 density it is possible to estimate (independent of the specific V^{3+} distribution at higher concentrations) the radius of the black sphere around this ion.

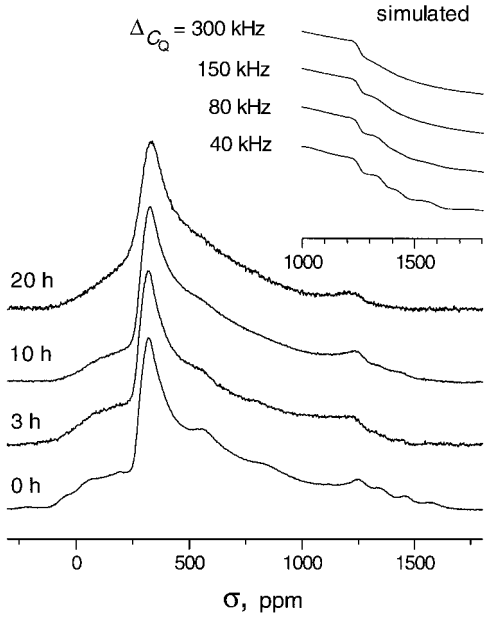

Figure 7. Wide line one-pulse 105.25 MHz ^{51}V NMR spectra of V_2O_5 milled for different times: (a) 0 h; (b) 3 h; (c) 10 h; (d) 20 h. Simulated one-pulse spectra (data set 1 from Table 1) with quadrupolar constant C_Q distributed around 799 kHz in a Gaussian-like fashion: (e) ΔC_Q = 40 kHz; (f) ΔC_Q = 80 kHz; (g) ΔC_Q = 150 kHz; (h) ΔC_Q = 300 kHz.

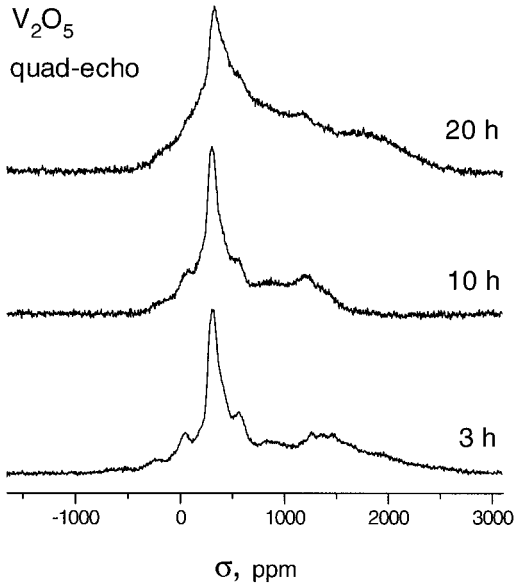

Figure 8. Wide line quadrupolar-echo ^{51}V NMR spectra of V_2O_5 milled for different times: (a) 3 h; (b) 10 h; (c) 20 h recorded at 105.25 MHz with t_1 = 55 μs and t_2 = 57 μs.

It is assumed that the NMR signal of any V^{5+} ion in this sphere is unobservable due to the paramagnetic line broadening and fast nuclear magnetic relaxation. This rough estimate gives a value of approximately 10 Å for the sphere radius. Because of the weak (inverse cubic root) dependence of the sphere radius on the curve slope, the value of the radius is not very sensitive to possible errors in the V^{3+} concentration. We thus believe that the above estimate of 10 Å is correct within a factor of about two.

Conclusions

The results presented in this paper permit us to draw the following conclusions on the local environment of vanadium nuclei in V_2O_5 powder after grinding.

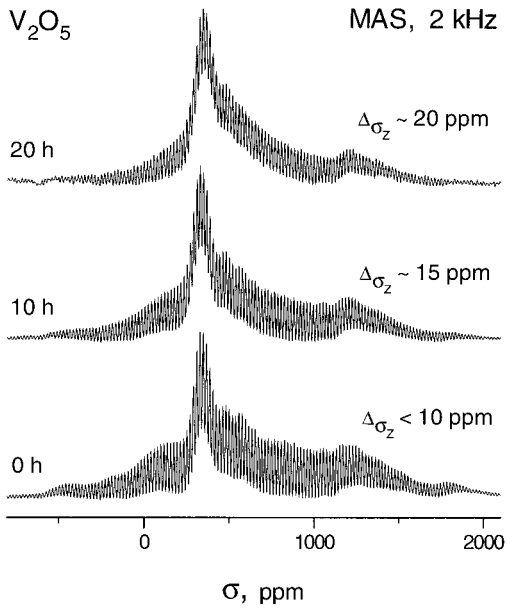

Figure 9. Experimental ^{51}V MAS NMR spectra of V_2O_5 milled for different times: (a) 0 h; (b) 10 h; (c) 20 h recorded at ν_r = 2.0 kHz.

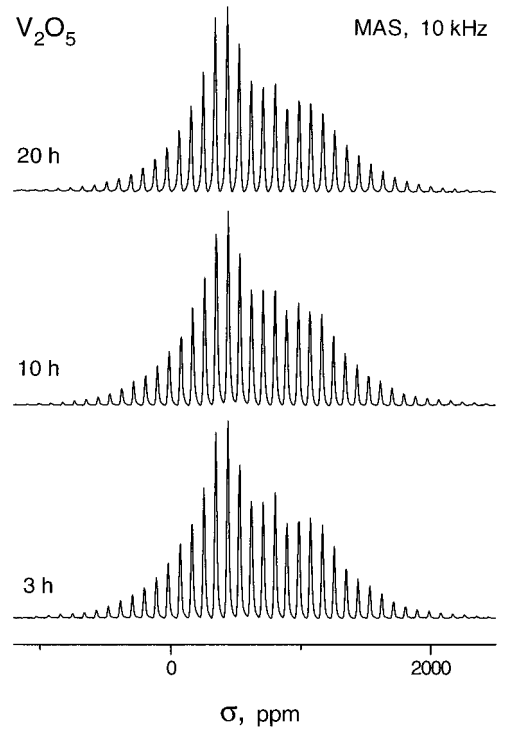

Figure 10. Experimental ^{51}V MAS NMR spectra of V_2O_5 milled for different times: (a) 3 h; (b) 10 h; (c) 20 h recorded at ν_r = 10.0 kHz.

TABLE 3: Concentrations of V^{3+} and V^{4+} and Relative Intensities of Central NMR Transitions for Milled V_2O_5 Samples

milling time/h	$[V^{3+}] \times 10^{20}$, g^{-1}	$[V^{4+}] \times 10^{20}$, g^{-1}	central NMR transition relative intensity
0	1.4	1.3	1
3	2.2	1.7	0.60
10	2.5	1.2	0.53
20	4.3	4.0	0.27

(1) Most of the vanadium atoms in milled V_2O_5 are in the V^{5+} state, with the concentrations of V^{4+} and V^{3+} being small. They are increasing with the milling time.

(2) V^{4+} and V^{3+} ions are most likely distributed inhomoge-

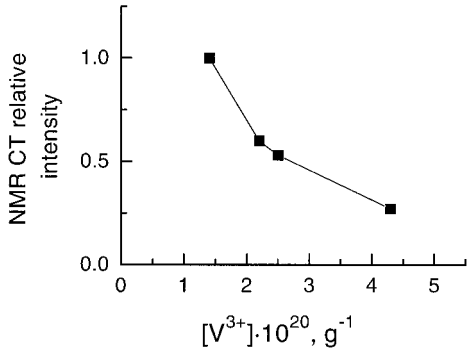

Figure 11. Intensity of central transition in ^{51}V NMR spectra of V_2O_5 as a function of V^{3+} ion concentration in milled samples (see Table 2).

neously. There is no significant influence of paramagnetic V^{4+} on the local environment of V^{5+} in large agglomerates of V_2O_5 presumably because the V^{4+} is located in small patches of V_6O_{13}-like shear structures.

(3) For 20 h milled samples of V_2O_5 only a small part of the V^{5+} ions have characteristic NMR features typical for well crystalline V_2O_5. The local environment of the vanadium sites is more strongly distorted when compared with polycrystalline V_2O_5.

(4) Paramagnetic V^{3+} ions are responsible for the loss (up to about 70%) of intensity in ^{51}V NMR spectra. The influence of V^{4+} paramagnetic ions is significantly smaller.

(5) No V^{5+} ions in tetrahedral coordination are formed during grinding.

Acknowledgment. This investigation has been supported by the Russian Foundation for Basic Research (Grant RFBR 98-03-32323). Work done in Munich was financially supported by the Deutsche Forschungsgemeinschaft and by the Fonds der Chemischen Industrie. The cooperation between the two research groups was made possible by an agreement between the Deutsche Forschungsgemeinschaft and the Russian Academy of Sciences.

References and Notes

(1) Che, M.; Bonneviot, L. *Z. Phys. Chem. Neue Folge* **1987**, *152*, 113.

(2) Sobalik, Z.; Lapina, O. B.; Mastikhin, V. M. In *Preparation of Catalysts V*; Poncelet, G., Jacobs, P. A., Grange, P., Delmon, B., Eds.; Elsevier: Amsterdam, 1991; p 507.

(3) Sobalik, Z.; Lapina, O. B.; Novgorodova, O. N.; Mastikhin, V. M. *Appl. Catal.* **1990**, *63*, 191.

(4) Knözinger, H.; Taglauer, E. *Catalysis*; The Royal Society of Chemistry: London, 1993; Vol. 10; p 1.

(5) Ziolkowski, J.; Kozlowski, R.; Mocala, K.; Haber, J. *J. Solid State Chem.* **1980**, *35*, 297.

(6) Haber, J. *Pure Appl. Chem.* **1984**, *56*, 1663.

(7) Haber, J.; Machej, T.; Czeppe, T. *Surf. Sci.* **1985**, *151*, 301.

(8) Knözinger, H.; Taglauer, E. In *Handbook of Heterogeneous Catalysis*; Wiley-VCH: Weinheim, 1997; Vol. 1, p 216.

(9) Mestl, G.; Verbruggen, N. F. D.; Lange, F. C.; Tesche, B.; Knözinger, H. *Langmuir* **1996**, *12*, 1817.

(10) Heinicke, G.; *Tribochemistry*; Carl Hanser Verlag: München, Wien, 1984.

(11) Mestl, G.; Knözinger, H. *Langmuir* **1998**, *14*, 3964.

(12) Eckert, H.; Wachs, I. *J. Phys. Chem.* **1989**, *93*, 6796.

(13) Lapina, O. B.; Mastikhin, V. M.; Shubin, A. A.; Krasilnikov, V. V.; Zamaraev, K. I. *Prog. Nucl. Magn. Reson. Spectrosc.* **1992**, *24*, 457.

(14) Mastikhin, V. M.; Lapina, O. B. *Vanadium Catalysts: Solid State NMR, in NMR Encyclopedia* **1996**, *8*, 10771.

(15) Skibsted, J.; Nielsen, N. C.; Bildsoe, H.; Jakobsen, H. J. *Chem. Phys. Lett.* **1992**, *188*, 405.

(16) Skibsted, J.; Nielsen, N. C.; Bildsoe, H.; Jakobsen, H. J. *J. Am. Chem. Soc.* **1993**, *115*, 7351.

(17) Jager, C. *NMR: Basic Princ. Prog.* **1994**, *31*, 133.

(18) Fernandez, C.; Bodart, P.; Amoureux, J. P. *Solid State NMR* **1994**, *3*, 79.

(19) Skibsted, J.; Vosegaard, T.; Bildsoe, H.; Jakobsen, H. *J. Am. Chem. Soc.* **1996**, *100*, 14872.

(20) Amoureux, J. P.; Fernandez, C.; Carpentier, L.; Cochon, E. *Phys. Status Solidi A* **1992**, *132*, 461.

(21) Frydman, L.; Harwood, J. S. *J. Am. Chem. Soc.* **1995**, *117*, 5367.

(22) Amoureux, J.-P.; Fernandez, C.; Frydman, L. *Chem. Phys. Lett.* **1996**, *259*, 347.

(23) Brown, S. P.; Heyes, S. J.; Wimperis, S. *J. Magn. Reson. Series A* **1996**, *119*, 289.

(24) Jakobsen, H. J.; Daugaard, P.; Langer, V. *J. Magn. Reson.* **1988**, *76*, 162.

(25) Shubin, A. A.; Lapina, O. B.; Zhidomirov, G. M. IXth AMPERE Summer School, Abstracts, Novosibirsk, USSR, 20−26, September 1987; p 103.

(26) Herzfeld, J.; Berger, A. E. *J. Chem. Phys.* **1980**, *73*, 6021.

(27) Berry, F. J. *Inorg. Chim. Acta* **1983**, *76*, L205.

(28) Haase, J.; Oldfield, E. *J. Magn. Reson. Ser. A* **1993**, *101*, 30.

(29) Man, P. P. *Phys. Rev. B.* **1995**, *52*, 9418.